

Article

A New Criterion for the Splashing of a Droplet on Dry Surface from High-Fidelity Simulations

Shijie Jiang ¹, Hongbing Xiong ¹ , Baolin Tian ² and Zhaosheng Yu ^{1,*} 
¹ State Key Laboratory of Fluid Power and Mechatronic Systems, Department of Mechanics, Zhejiang University, Hangzhou 310027, China; 3180101280@zju.edu.cn (S.J.); hbxiong@zju.edu.cn (H.X.)

² School of Aeronautic Science and Engineering, Beihang University, Beijing 100191, China; tianbaolin@buaa.edu.cn

* Correspondence: yuzhaosheng@zju.edu.cn

Abstract: In this study, a new criterion for the splashing of a droplet on a dry smooth surface is established from high-fidelity numerical simulations. The new criterion involves the Weber number, Reynolds number and contact angle. A new splashing mode, termed spreading splashing, is proposed, which predominates for contact angles below 120 degrees. For contact angles above 120 degrees, prompt splashing dominates. For contact angles above 90 degrees, there exists a critical Weber number of around 60, below which splashing does not occur.

Keywords: droplet; splashing; criterion

1. Introduction

The impact of liquid droplets on a solid surface is widely encountered in nature and industrial applications [1]. For instance, the impingement of supercooled water on the surface of aircraft wings and subsequent icing is one of the primary factors leading to aviation accidents [2]. During the spray cooling process, the impact of liquid droplets on a heated surface or a thin liquid film results in heat exchange, which predominantly determines the cooling efficiency of heating elements or heated surfaces. The injection state, surface tension, liquid viscosity, and spreading behavior of micro-droplets during inkjet spraying are crucial factors for the quality of printed materials.

The impact of liquid droplets on a surface is a highly intricate fluid dynamics process, involving the interaction of gas–liquid two-phase flow, wall contact line dynamics, and liquid–solid interfacial interactions. Various morphological changes occur in this process, including spreading, deposition, splashing, and rebound. These transformations are closely associated with droplet characteristics such as liquid viscosity, density, surface tension, diameter, impact velocity, and temperature. Additionally, they are influenced by surface properties such as morphology, temperature, roughness, wettability (hydrophobic and hydrophilic characteristics), and surface structure [3–6]. The inertia force, viscous force, and surface tension are involved in the impacting process, and consequently the impact dynamics can be controlled by the Reynolds and Weber numbers, defined as

$$Re = \frac{\rho D_0 V_0}{\mu}, \quad We = \frac{\rho D_0 V_0^2}{\sigma}, \quad (1)$$

where ρ is the liquid density, D_0 is the initial diameter of the droplet, V_0 is the impact velocity of the droplet, μ is the liquid viscosity, and σ is the surface tension coefficient. Alternatively, the Ohnesorge and capillary numbers may be used, which are related to the Reynolds and Weber numbers via

$$Oh = \frac{\mu}{\sqrt{\rho \sigma D_0}} = \frac{\sqrt{We}}{Re}, \quad Ca = \frac{\mu V_0}{\sigma} = \frac{We}{Re}. \quad (2)$$



Citation: Jiang, S.; Xiong, H.; Tian, B.; Yu, Z. A New Criterion for the Splashing of a Droplet on Dry Surface from High-Fidelity Simulations. *Appl. Sci.* **2024**, *14*, 8553. <https://doi.org/10.3390/app14188553>

Academic Editor: Sergey Suslov

Received: 13 August 2024

Revised: 8 September 2024

Accepted: 20 September 2024

Published: 23 September 2024



Copyright: © 2024 by the authors. Licensee MDPI, Basel, Switzerland. This article is an open access article distributed under the terms and conditions of the Creative Commons Attribution (CC BY) license (<https://creativecommons.org/licenses/by/4.0/>).

The morphology of liquid droplets undergoes significant changes in splashing, often breaking into numerous secondary droplets that move far away from the point of impact. Hence, it is of significant importance to determine whether splashing occurs in engineering applications. For numerical simulations of the flow laden with spray droplets using the Euler–Lagrange method [7], the splashing criterion may be used to determine whether a droplet would deposit on the wall or splash into smaller droplets.

Extensive studies on droplet splashing have been conducted. Over a century ago, Worthington [8–10] undertook pioneering studies on droplet splashing. He summarized and categorized a series of states that occur after droplets collide with a surface. He experimentally observed the splashing of large milk and mercury droplets impacting on a smooth glass surface, although he did not observe corona splashing, which is characterized by the formation of a crown-shaped lamella up in the air. The experimental results of Engel et al. [11] and Levin and Hobbs [12] showed that increasing surface roughness caused liquid droplets to be more prone to corona splashing, and splashing without a crown formation occurred only on extremely smooth surfaces. Based on their experiments, Stow and Hadfield [13] were the first to propose an empirical formula for the splashing threshold, expressed as $K = We^{0.5} Re^{0.25}$. When K exceeds the critical value K_c , splashing occurs. Mundo et al. [14] investigated the impact of small water droplets on relatively rough surfaces and obtained the critical value K_c of 57.7. Wachters and Westerling [15] observed the onset of splashing at a critical Weber number $We_c = 80$ for a number of different liquids impacting a polished gold surface, and correlated the splashing threshold with the critical Weber number. Range and Feuillebois [16] examined the effects of wall roughness on droplet impact at low Oh number, and correlated the critical Weber number for the onset of splashing with the following expression:

$$We_c = a[\ln(R_a^*)]^b, \quad (3)$$

where a and b are two parameters whose values depend on the droplet and solid surface properties, R_a^* is the non-dimensional average wall roughness defined as Ra/D_0 , and R_a is the dimensional average roughness. Wal et al. [17] proposed a simple criterion, $\sqrt{Ca} = We^{0.5} Re^{-0.5} = 0.35$, to distinguish between the splashing and non-splashing modes. Quetzeri-Santiago et al. [18] conducted a study on the splashing behavior of droplets impacting on various substrates with different wetting properties. They observed that the maximum dynamic advancing contact angle and the splashing ratio β effectively characterized the splashing behavior. Roisman et al. [19] conducted experiments to investigate the splashing behavior of liquid droplets impacting dry surfaces with varying roughness. The results indicated that the criterion $K = We^{0.5} Re^{0.25}$ failed to accurately predict the splashing threshold for dry surfaces with different roughness levels. Li et al. [20] proposed a new splashing criterion $(WeRe)^{0.25} > 25.15$ for a superhydrophobic surface with the contact angle $CA = 156^\circ$, based on their numerical simulation results. Zhang et al. [21] experimentally investigated the dynamic behavior of water droplets impacting on surfaces with various wettabilities (ranging from hydrophilic to superhydrophobic), and proposed a criterion as $K/K_0 = 1 + \alpha \cos \theta_a$, where θ_a is the advancing contact angle, α is a constant, and K_0 is the criterion value without consideration of contact angle.

To summarize, various criteria on droplet splashing have been proposed; however, they are inconsistent with each other and there has been no consensus on the splashing criterion. The criterion proposed by Li et al. [20] is the only one established from numerical simulations, to our knowledge. This criterion is only for a fixed contact angle $CA = 156^\circ$. The aim of the present study is to propose a splashing criterion accounting for the effects of the contact angle from high-fidelity numerical simulations. The volume of fluid (VOF) method was employed to capture the liquid–gas interface and the direct numerical simulation (DNS) method was applied for solving the three-dimensional incompressible Navier–Stokes equations. Simulations of droplet impacts on surfaces with different wettabilities and liquid properties were conducted, covering a wide range of CA (40–160), Re (500–6500), and We (40–300). Various modes of droplet impingement, including spread-

ing and different types of splashing, were identified. Splashing is precisely defined and a novel splashing mode, termed spreading splashing, is identified and characterized. A new splashing model for different contact angles is proposed.

2. Numerical Method

The two-fluid model, the mixture model and the interface-tracking method are typically used for the simulation of gas–liquid two-phase flows [22]. The VOF method is an interface-tracking approach used to model two or more immiscible fluids in the Eulerian frame. For the issue of droplet splashing, mass conservation is crucial, and the primary advantage of the Volume-of-Fluid (VOF) method lies in its excellent mass conservation. This method employs a set of momentum equations shared by incompatible fluid components and tracks the interface in the computational domain by introducing the target fluid volume fraction. In the present study, we employ an open-source code Basilisk [23,24] for numerical simulations. Basilisk supports Adaptive Mesh Refinement (AMR) techniques, enabling the automatic adjustment of grid resolution based on flow field characteristics. Based on a criterion of wavelet-estimated discretization error [25], Basilisk allows for increased grid resolution in regions requiring finer description and reduced grid resolution in other areas according to all important variables, thereby achieving efficient simulations. It is also designed with a better structure to enhance parallel running efficiency. Based on these characteristics, Basilisk is well-suited for addressing the issue of droplet collision, since accurate capturing of the intricate structures that emerge during droplet collision needs substantial computational resources. The reader is referred to [23,24] for details of the method. Basilisk has been widely applied to various droplet problems [26–30].

3. Physical Model and Numerical Method Validation

3.1. Physical Model

We adopted a cubic computational domain with a side length L of 15 mm. At a distance of 3 mm from the center to the wall, we placed a liquid droplet with a diameter of D_0 and an initial velocity V_0 in the downward vertical direction, as illustrated in Figure 1.

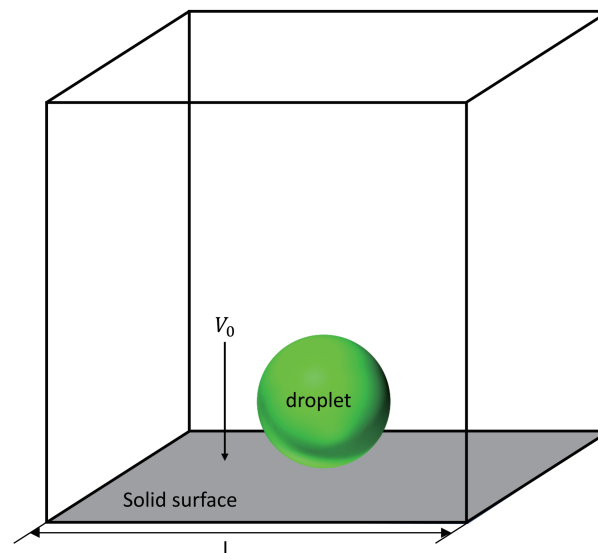


Figure 1. Schematic illustration of the computational domain.

Since we are mainly concerned with the splashing, for which the collision velocity is large and the collision time is short, the influence of gravity is neglected.

3.2. Numerical Method Validation

To validate the accuracy of our numerical simulation, we compared our simulation results to the numerical and experimental results from Li et al. [20]. The simula-

tion settings are as follows: initial diameter of droplet $D_0 = 2.14$ mm, initial velocity of droplet $V_0 = 0.64$ m/s, contact angle $CA = 156^\circ$, density of liquid $\rho_l = 998$ kg/m³, density of gas $\rho_g = 1.185$ kg/m³, viscosity of liquid $\mu_l = 8.89 \times 10^{-4}$ Pas, viscosity of gas $\mu_g = 1.84 \times 10^{-5}$ Pas, and surface tension coefficient $\sigma = 0.0728$ N/m. No slip boundary condition was adopted for the solid bottom surface, and pressure outlet boundary conditions were adopted for other surfaces.

The grid of the computational domain is initialized to a resolution of level 6, which means that the minimum grid size is $1/2^6$ of the side length of the simulation domain. During the computation process, we dynamically adjust the grid based on the velocity and the volume fraction α . Grid refinement is applied to regions with high velocity gradients and significant changes in the volume fraction (near the gas–liquid interface), with a maximum refinement level set to 10. Conversely, grid resolution is reduced in other regions (far from the impact area), as shown in Figure 2. The maximum number of the grids is typically around 10 million for most cases and is around 50 million for a few cases, resulting in a huge computational cost for the present study. A higher refinement level is limited by our computational resources.

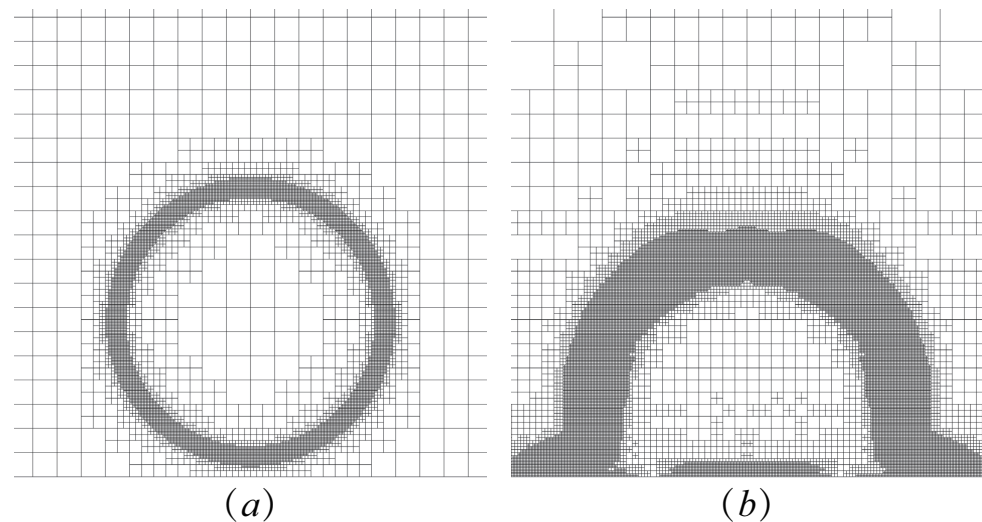


Figure 2. Spatial resolutions: (a) $t = 0$ ms; (b) $t = 0.8$ ms.

Figure 3 depicts a comparative illustration of the different stages of droplet–wall interaction. From the figure, it is evident that the numerical simulation in the present study faithfully reproduces the behavior of the droplet impacting the wall, with the shape of the droplet in the simulation closely matching the experimental observations. At the onset of collision, the droplet exhibits an incomplete spherical shape, gradually spreading into a pancake-like morphology until reaching its maximum diameter. Subsequently, the droplet recoils and rebounds before finally detaching from the surface. Notably, during the spreading phase of the droplet, pronounced capillary waves appear on the upper half of the droplet surface due to surface tension, a detail not captured in the simulation results of Li et al. [20], highlighting the accuracy of our simulations.

The non-dimensional time is defined as

$$t^* = \frac{Ut}{D_0} \quad (4)$$

In order to quantify the simulation results, the non-dimensional parameter spreading factor ζ is defined as

$$\zeta(t) = \frac{D(t)}{D_0} \quad (5)$$

where $D(t)$ is the diameter of the wetted area during the impact process.

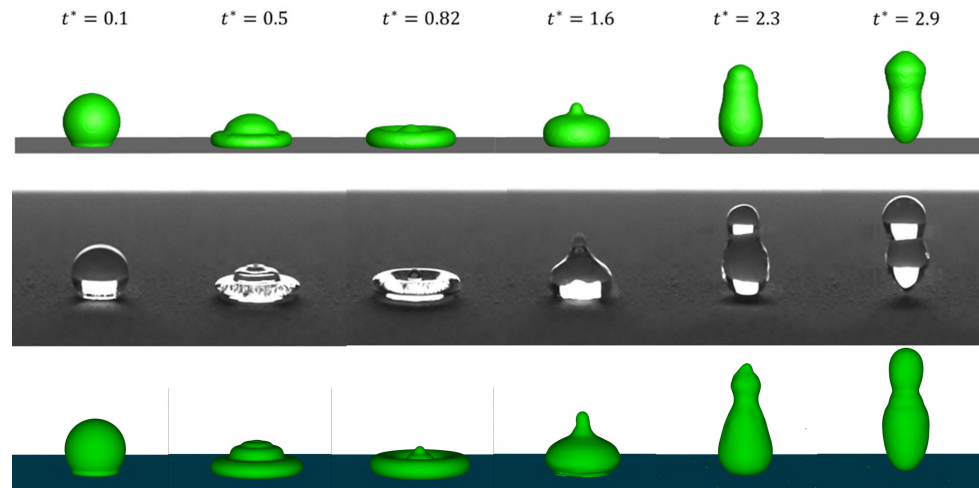


Figure 3. Comparison of the droplet impact behaviors. Top: simulation results of Li et al. [20]. Middle: experimental results of Li et al. [20]. Bottom: present simulation results ($D_0 = 2.14$ mm, $V_0 = 0.64$ m/s).

As can be seen from Figure 4, both our simulation results and those of Li et al. [20] are in good agreement with the experimental results. The final spreading factor ξ values for our simulation, Li et al. [20], and the experiments are 1.432, 1.42, and 1.428, respectively. The relative deviation between our simulation and the experiments is only around 0.28%.

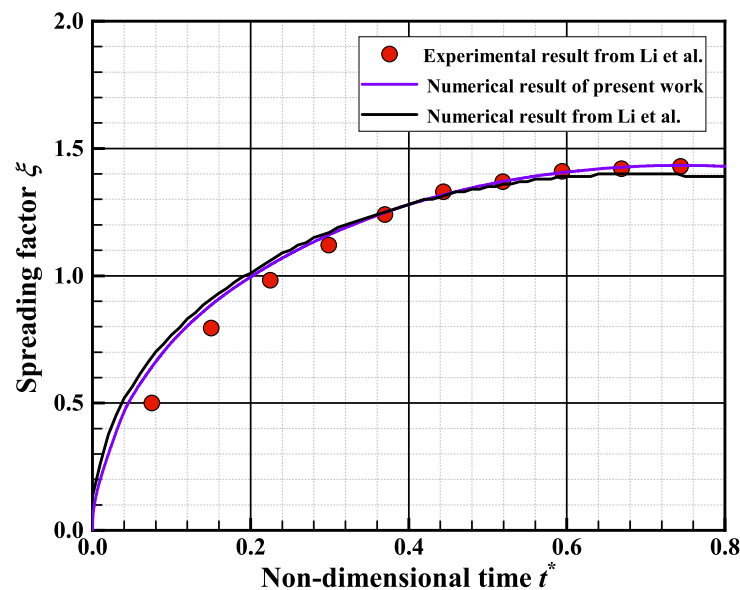


Figure 4. Comparison of the spreading factor between the present work and Li et al. [20].

4. Results and Discussion

We use the same simulation settings in the above validation problem, except that we vary the droplet viscosity, the surface tension coefficient, and the contact angle to obtain different Reynolds numbers (500–6500), Weber numbers (60–250), and contact angles (40°–160°). For experiments, it might be more convenient to vary the impact velocity and the droplet diameter to obtain different Reynolds and Weber numbers. However, changes to the impact velocity or the droplet diameter lead to changes to both Reynolds and Weber numbers. The reason why we vary the droplet viscosity and the surface tension coefficient is that the Reynolds and Weber numbers can be changed independently, which can help to determine their individual effects, such as the critical Weber number discussed later. Due to the limitation of the computational resource, the effects of the gas properties, which

might be measured by dimensionless quantities such as the liquid–gas viscosity and density ratios, are not investigated.

4.1. Modes of Droplet Impact

In our simulations, various modes of droplet impacting are observed, including spreading, fingering, receding breakup, partial spreading splash, splash, partial prompt splash, and prompt splash, as shown in Figure 5.

Due to the primary focus of this study being on the criterion for droplet splashing, in order to obtain more precise splashing thresholds, the control parameters (We , Re) are set around the vicinity of the droplet-splashing threshold. This allows us to reveal new modes of splashing from the simulation results. Definitions of splashing in previous works have been vague. To better identify the modes of droplet behavior after collision, we propose the following precise definition of droplet splashing based on the simulation results.

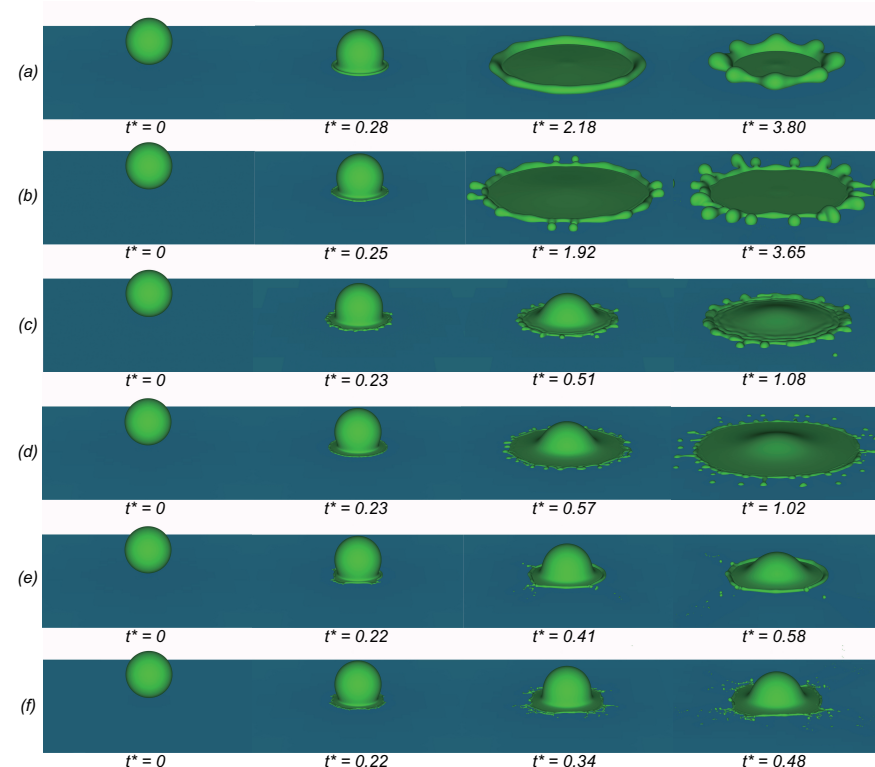


Figure 5. Outcomes of droplet impact for $D_0 = 2.6$ mm, $V_0 = 1$ m/s. (a) Spreading: $CA = 150^\circ$, $Re = 500$, $We = 100$; (b) receding breakup: $CA = 120^\circ$, $Re = 1000$, $We = 120$; (c) partial spreading splash: $CA = 90^\circ$, $Re = 6500$, $We = 60$; (d) spreading splash: $CA = 60^\circ$, $Re = 1000$, $We = 120$; (e) partial prompt splash: $CA = 150^\circ$, $Re = 1000$, $We = 100$; (f) prompt splash: $CA = 150^\circ$, $Re = 1000$, $We = 120$.

The generation of secondary droplets before the droplet reaches its maximum diameter is defined as splashing, as shown in Figure 5c–f. Based on the distribution, morphology, and generation time of the secondary droplets, splashing can be further categorized into partial spreading splashing (late generation time of secondary droplets, relatively large droplet diameter, fewer in number and asymmetric distribution), spreading splashing (late generation time of secondary droplets, relatively large diameter, fewer in number and symmetric distribution), prompt splashing (short time interval for secondary droplet generation after collision, small droplet diameter, more in number, and symmetric distribution), and partial prompt splashing (short time interval for secondary droplet generation after collision, small droplet diameter, more in number, and asymmetric distribution). Crown splashing was not observed in our simulations. Note that we distinguish between spreading splashing and prompt splashing according to the difference described above. However, since prompt

splashing is not clearly defined in the literature, it is possible that both spreading and prompt splashing modes here belong to the prompt splashing mode in the literature.

In our simulations, both prompt splashing and partial prompt splashing occur only in cases where the contact angle exceeds 120° , while spreading splashing and partial spreading splashing do not occur for large contact angles ($CA > 120^\circ$). This implies that large contact angles (hydrophobic surfaces) would suppress spreading splashing and promote prompt splashing, while small contact angles (hydrophilic surfaces) would suppress prompt splashing and promote spreading splashing.

4.2. Critical Weber Number

During the analysis of the simulation results, we observed that for a contact angle greater than 90° , there exists a critical Weber number, We_c , such that when We is less than We_c , despite a large Reynolds number, the droplet does not undergo splashing, as depicted in Figure 6.

$Re=6500$, $We=60$

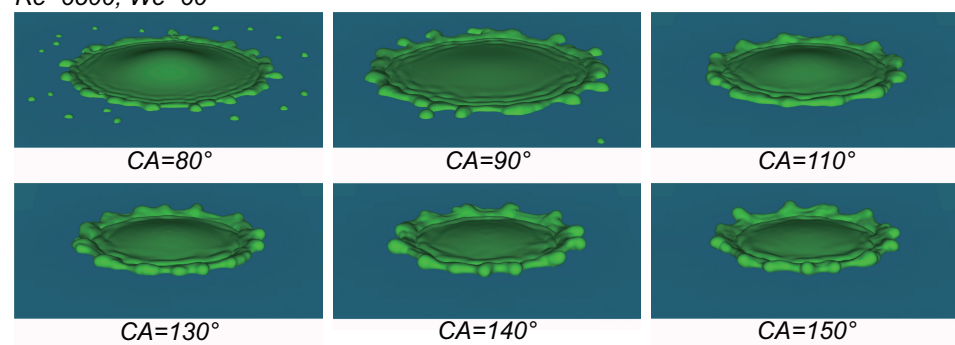


Figure 6. Droplet impact at different contact angles for $Re = 6500$ and $We = 60$.

When the contact angle is less than 90° , the predominant splashing type is spreading splashing. This splashing occurs mainly due to the rapid movement of the triple contact line of the droplet with a small contact angle. The kinetic energy at the droplet's edge is larger compared to the center, resulting in a velocity difference between the edge and the center, leading to detachment of the droplet at the edge. During the spreading process of the droplet, the viscous forces and surface tension collectively dissipate the droplet's kinetic energy. Therefore, both Reynolds and Weber numbers determine whether the droplet will splash. When the contact angle is greater than 90° , the primary splashing type is prompt splashing, occurring within a short time after collision. At this point, viscous forces contribute less to the dissipation of droplet kinetic energy, and the main influencing factors on splashing are surface tension and inertia. Hence, the Weber number has a greater effect on splashing than the Reynolds number. Therefore, as long as the Weber number is smaller than a certain value, splashing does not occur. From our simulation results, for the contact angle above 90° , the critical Weber number is around 60.

4.3. Criterion for Splashing

As mentioned in the Introduction, various criteria for the occurrence of splashing have been proposed. Although some of these criteria may conflict with each other, they share a common form represented by $K = ReWe^n$. Therefore, considering the critical Weber number, we define a critical parameter for splashing occurrence as follows:

$$K = (We - We_c)^{\frac{1}{n+1}} Re^{\frac{n}{n+1}} \quad (6)$$

where We_c is the critical Weber number, and n is a parameter.

By fitting to our data from 270 simulation cases, the parameter n is determined as follows:

$$n = \begin{cases} -0.02CA + 2.49, & \text{for } CA \leq 90^\circ \\ 1, & \text{for } CA > 90^\circ \end{cases} \quad (7)$$

From Equation (7), when the contact angle (CA) is less than or equal to 90° , there exists a good linear relationship between n and CA. However, when the contact angle exceeds 90° , n remains constant and is equal to unity. When the CA is small, the hindering effect of surface tension on droplet spreading is relatively weak because of the geometry of the edge of the droplet, and the viscous force dominates. In the spreading stage, the kinetic energy of the droplet is primarily dissipated by viscous forces, preventing the droplet's edge from having enough kinetic energy to overcome the surface tension and form secondary droplets. As CA increases, the geometry of the edge of the droplet changes, and thus the effect of surface tension gradually increases (the surface tension and viscous forces together dissipate the droplet's kinetic energy), leading to the decrease in n , which means that the relative importance of the Reynolds number to the Weber number decreases. n being 1 leads to $K = (We - We_c)^{\frac{1}{2}} Re^{\frac{1}{2}}$, which is consistent with the results of Li et al. [20], who established the criterion only for the contact angle $CA = 156^\circ$ and did not consider the critical Weber number. Since both the powers of We and Re are positive, an increase in the impact velocity, droplet size, or droplet density, or a decrease in the droplet viscosity or surface tension, would promote the occurrence of splashing.

To illustrate the effects of the contact angle on the splashing threshold K_c , we present the relationship between K_c and the contact angle CA in Figure 7. From the figure, for contact angles less than 90° , the value of K_c remains almost unchanged with variation in CA. However, for contact angles greater than 90° , the value of K_c decreases with increasing CA. This observation is consistent with the experimental results of Zhang et al. [21], indicating that the hydrophobic surface greatly promotes droplet splashing. Our value of K_c is smaller than those of Li et al. [20] and Zhang et al. [21]. This may be caused by the difference in judging the occurrence of splashing. In the present study, we deem it as splashing as long as any secondary droplet appears, which might not be observed or regarded as splashing in the experiments. In addition, the wall roughness and the properties of the surrounding gas that are not considered in the criterion may differ in different studies and result in discrepancy.

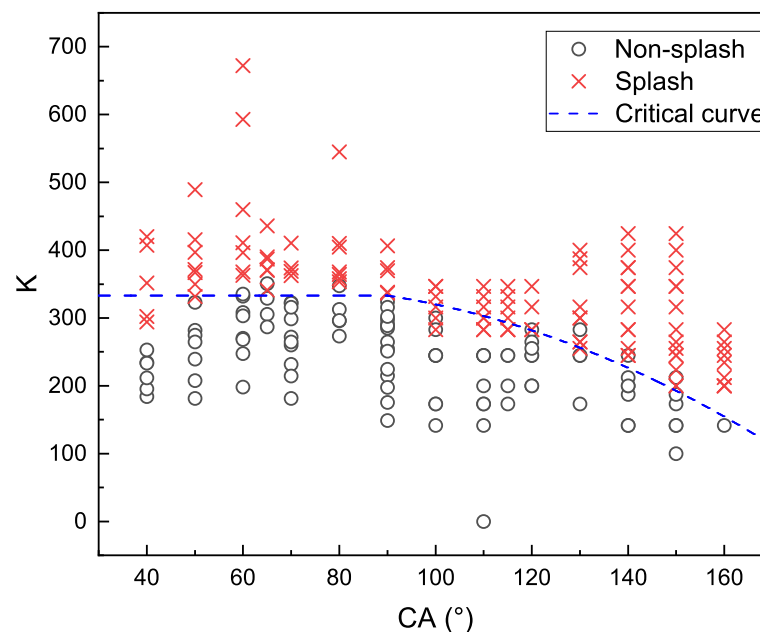


Figure 7. The splashing threshold K_c as a function of the contact angle. The blue line represents the critical curve obtained by Equation (8).

The critical value of K is determined from our data in Figure 7, as follows:

$$K_c = \begin{cases} 333, & \text{for } CA \leq 90^\circ \\ -0.021CA^2 + 2.7CA + 260, & \text{for } CA > 90^\circ \end{cases} \quad (8)$$

Figure 8 displays the phase diagrams in terms of the Weber and Reynolds numbers for different contact angles. It can be observed that our criteria (6)–(8) can effectively distinguish between splashing and non-splashing modes for a droplet impacting the wall at different contact angles, and there exists a critical Weber number for splashing at a CA above 90° .

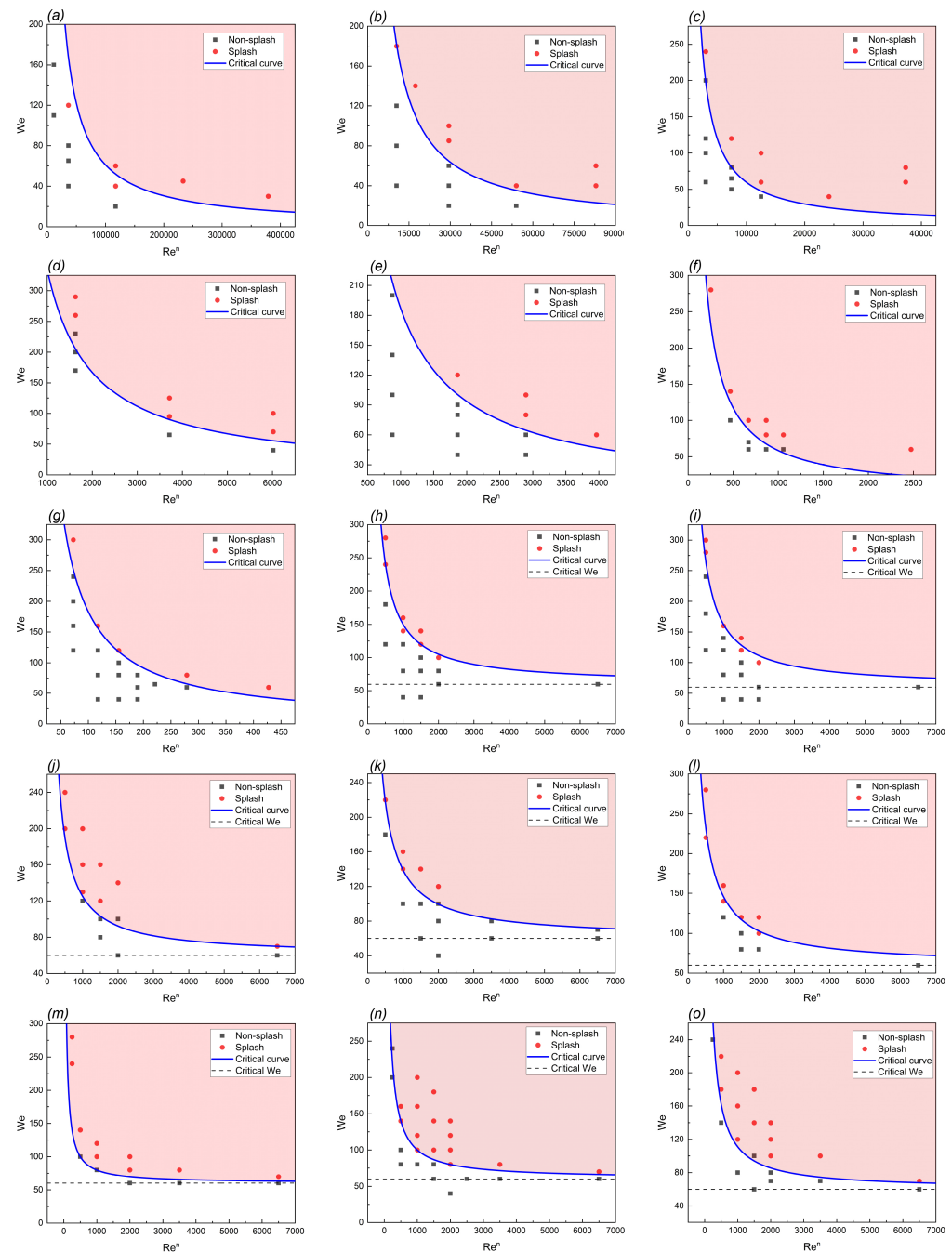


Figure 8. Phase diagrams in terms of the Weber and Reynolds numbers for different contact angles: (a) $CA = 40^\circ$; (b) $CA = 50^\circ$; (c) $CA = 60^\circ$; (d) $CA = 65^\circ$; (e) $CA = 70^\circ$; (f) $CA = 80^\circ$; (g) $CA = 90^\circ$; (h) $CA = 100^\circ$; (i) $CA = 110^\circ$; (j) $CA = 115^\circ$; (k) $CA = 120^\circ$; (l) $CA = 130^\circ$; (m) $CA = 140^\circ$; (n) $CA = 150^\circ$; (o) $CA = 160^\circ$. The lines represent our criteria (6)–(8).

5. Conclusions

Numerical simulations of a droplet impact on a surface with different wettabilities have been performed. The accuracy of our numerical simulations is validated through comparisons with experimental data from the literature. By varying the surface tension coefficient and viscosity of the droplet, we simulate the droplet–wall collisions near the splashing threshold at different Reynolds numbers (500–6500) and Weber numbers (60–250). The effects of surface wettability on the droplet-splashing threshold are investigated by changing the contact angle. Several typical modes of droplet impact are captured. A new spreading splashing mode is defined and a new criterion for splashing occurrence is established. The main findings are summarized as follows:

- (1) The phenomenon where secondary droplets are generated before the droplet spreads to its maximum diameter after collision is defined as splashing. Splashing with secondary droplets generated later, relatively larger in diameter, and fewer in number is defined as spreading splashing. Splashing with secondary droplets generated earlier, smaller in diameter, and greater in number is defined as prompt splashing. Based on the symmetry of the distribution of secondary droplets, splashing can be classified into partial splashing (asymmetric distribution of secondary droplets) and splashing (symmetric distribution of secondary droplets).
- (2) Spreading splashing primarily occurs in cases where the contact angle is relatively small ($CA \leq 120^\circ$), while prompt splashing prevails in situations where the contact angle is larger ($CA > 120^\circ$). An increase in the contact angle tends to inhibit spreading splashing, while promoting rapid splashing.
- (3) For contact angles greater than 90° , there exists a critical Weber number, We_c , below which splashing does not occur. From our simulations, $We_c \approx 60$.
- (4) Based on our results, a new criterion for splashing is proposed; $K_c = (We - We_c)^{\frac{1}{n+1}} Re^{\frac{n}{n+1}}$, where n equals $-0.02CA + 0.49$ for $CA \leq 90^\circ$ and 1 for $CA > 90^\circ$. For $CA \leq 90^\circ$, the threshold $K_c = 333$, and for $CA > 90^\circ$, $K_c = -0.021CA^2 + 2.7CA + 260$.

Our criterion for splashing is the first one that is established based on high-fidelity numerical simulations and accounts for the effects of contact angle. Due to some possible differences, such as the judgement of the splashing occurrence, the wall roughness, and the effects of the surrounding gas, quantitative agreement between our criterion and those in the literature was not reached. Our criterion corresponds to cases where the wall is smooth, and the Reynolds and Weber numbers are varied by changing the droplet viscosity and the surface tension coefficient, while the gas viscosity and density are fixed. The effects of the gas properties, which might be measured by dimensionless quantities such as the liquid–gas viscosity and density ratios, are not investigated. This is a good subject for future study. The criteria in the literature are also inconsistent with each other. We think that our criterion is a useful complement to the existing ones.

Author Contributions: Conceptualization, Z.Y., H.X. and B.T.; methodology, S.J. and H.X.; formal analysis, S.J., H.X., B.T. and Z.Y.; investigation, S.J., H.X., B.T. and Z.Y.; writing—original draft preparation, S.J.; writing—review and editing, Z.Y.; supervision, Z.Y.; funding acquisition, Z.Y. and B.T. All authors have read and agreed to the published version of the manuscript.

Funding: This research was funded by Key Laboratory of Computational Physics, Beijing Institute of Applied Physics and Computational Mathematics, and the National Natural Science Foundation of China (Grant No. 12332015, 12072319).

Institutional Review Board Statement: Not applicable.

Informed Consent Statement: Not applicable.

Data Availability Statement: The raw data supporting the conclusions of this article will be made available by the authors on request.

Conflicts of Interest: The authors declare no conflicts of interest.

Abbreviations

The following abbreviations are used in this manuscript:

VOF	Volume of Fluid
CSF	Continuum Surface Tension Force
AMR	Adaptive Mesh Refinement
CA	Contact Angle

References

1. Yarin, A.L. Drop impact dynamics: Splashing, spreading, receding, bouncing. *Annu. Rev. Fluid Mech.* **2006**, *38*, 159–192. [\[CrossRef\]](#)
2. Zhu, C.X.; Tao, M.J.; Zhao, N.; Zhu, C.L.; Wang, Z.Z. Study of droplet shadow zone of aircraft wing with diffusion effects. *AIAA J.* **2019**, *57*, 3339–3348. [\[CrossRef\]](#)
3. Stevens, C.S.; Latka, A.; Nagel, S.R. Comparison of splashing in high-and low-viscosity liquids. *Phys. Rev. E* **2014**, *89*, 063006. [\[CrossRef\]](#)
4. Xu, L. Liquid drop splashing on smooth, rough, and textured surfaces. *Phys. Rev. E* **2007**, *75*, 056316. [\[CrossRef\]](#) [\[PubMed\]](#)
5. Aboud, D.G.; Kietzig, A.M. Splashing threshold of oblique droplet impacts on surfaces of various wettability. *Langmuir* **2015**, *31*, 10100–10111. [\[CrossRef\]](#)
6. Josserand, C.; Thoroddsen, S.T. Drop impact on a solid surface. *Annu. Rev. Fluid Mech.* **2016**, *48*, 365–391. [\[CrossRef\]](#)
7. Owen, L.D.; Ge, W.; Rieth, M.; Arienti, M.; Esclapez, L.; Soriano, B.S.; Mueller, M.E.; Day, M.; Sankaran, R.; Chen, J.H. PeleMP: The Multiphysics Solver for the Combustion Pele Adaptive Mesh Refinement Code Suite. *J. Fluids Eng.* **2024**, *146*, 041103. [\[CrossRef\]](#)
8. Worthington, A.M. XXVIII. On the forms assumed by drops of liquids falling vertically on a horizontal plate. *Proc. R. Soc. Lond.* **1877**, *25*, 261–272.
9. Worthington, A.M. III. A second paper on the forms assumed by drops of liquids falling vertically on a horizontal plate. *Proc. R. Soc. Lond.* **1877**, *25*, 498–503.
10. Worthington, A.M. *The Splash of a Drop*; Society for Promoting Christian Knowledge: London, UK, 1895.
11. Engel, O.G. Waterdrop collisions with solid surfaces. *J. Res. Natl. Bur. Stand.* **1955**, *54*, 281–298. [\[CrossRef\]](#)
12. Levin, Z.; Hobbs, P.V. Splashing of water drops on solid and wetted surfaces: Hydrodynamics and charge separation. *Philos. Trans. R. Soc. Lond. Ser. A Math. Phys. Sci.* **1971**, *269*, 555–585.
13. Stow, C.D.; Hadfield, M.G. An experimental investigation of fluid flow resulting from the impact of a water drop with an unyielding dry surface. *Proc. R. Soc. Lond. A Math. Phys. Sci.* **1981**, *373*, 419–441.
14. Mundo, C.; Sommerfeld, M.; Tropea, C. Droplet-wall collisions: Experimental studies of the deformation and breakup process. *Int. J. Multiph. Flow* **1995**, *21*, 151–173. [\[CrossRef\]](#)
15. Wachters, L.; Westerling, N. The heat transfer from a hot wall to impinging water drops in the spheroidal state. *Chem. Eng. Sci.* **1966**, *21*, 1047–1056. [\[CrossRef\]](#)
16. Range, K.; Feuillebois, F. Influence of surface roughness on liquid drop impact. *J. Colloid Interface Sci.* **1998**, *203*, 16–30. [\[CrossRef\]](#)
17. Wal, R.L.V.; Berger, G.M.; Mozes, S.D. The splash/non-splash boundary upon a dry surface and thin fluid film. *Exp. Fluids* **2006**, *40*, 53–59. [\[CrossRef\]](#)
18. Quetzeri-Santiago, M.A.; Yokoi, K.; Castrejón-Pita, A.A.; Castrejón-Pita, J.R. Role of the dynamic contact angle on splashing. *Phys. Rev. Lett.* **2019**, *122*, 228001. [\[CrossRef\]](#)
19. Roisman, I.V.; Lembach, A.; Tropea, C. Drop splashing induced by target roughness and porosity: The size plays no role. *Adv. Colloid Interface Sci.* **2015**, *222*, 615–621. [\[CrossRef\]](#)
20. Li, W.; Wang, J.; Zhu, C.; Tian, L.; Zhao, N. Numerical investigation of droplet impact on a solid superhydrophobic surface. *Phys. Fluids* **2021**, *33*, 063310. [\[CrossRef\]](#)
21. Zhang, H.; Zhang, X.; Yi, X.; He, F.; Niu, F.; Hao, P. Effect of wettability on droplet impact: Spreading and splashing. *Exp. Therm. Fluid Sci.* **2021**, *124*, 110369. [\[CrossRef\]](#)
22. Mushtaq, M.U.; Bibi, M.; Mehmood, R.; Amin, M.; Sanaullah, K.; Iqbal, A. Correction: Fluid Dynamics Technique in Membrane Bioreactor Systems. *Arch. Comput. Methods Eng.* **2024**, *31*, 551. [\[CrossRef\]](#)
23. Popinet, S. Gerris: A tree-based adaptive solver for the incompressible Euler equations in complex geometries. *J. Comput. Phys.* **2003**, *190*, 572–600. [\[CrossRef\]](#)
24. Popinet, S. An accurate adaptive solver for surface-tension-driven interfacial flows. *J. Comput. Phys.* **2009**, *228*, 5838–5866. [\[CrossRef\]](#)
25. Van Hooff, J.A.; Popinet, S.; Van Heerwaarden, C.C.; Van der Linden, S.J.; De Roode, S.R.; Van de Wiel, B.J. Towards adaptive grids for atmospheric boundary-layer simulations. *Bound.-Layer Meteorol.* **2018**, *167*, 421–443. [\[CrossRef\]](#)
26. García-Geijo, P.; Riboux, G.; Gordillo, J. The skating of drops impacting over gas or vapour layers. *J. Fluid Mech.* **2024**, *980*, A35. [\[CrossRef\]](#)
27. Ray, S.; Han, Y.; Cheng, S. Pinch-off dynamics in unequal-size droplets head-on collision on a wetting surface: Experiments and direct numerical simulations. *Phys. Fluids* **2023**, *35*, 104955. [\[CrossRef\]](#)

28. Liu, L.; Guan, X.; Fu, Q. Numerical simulation study of extensional characteristics impacts on the viscoelastic thread deformation and satellite droplet generation. *J. Non-Newton. Fluid Mech.* **2023**, *311*, 104955. [[CrossRef](#)]
29. Pan, Y.; Wang, Z.; Zhao, X.; Deng, W.; Xia, H. On axisymmetric dynamic spin coating with a single drop of ethanol. *J. Fluid Mech.* **2022**, *951*, A30. [[CrossRef](#)]
30. Li, Y.; Xu, Z.; Peng, X.; Wang, T.; Che, Z. Numerical simulation of secondary breakup of shear-thinning droplets. *Phys. Fluids* **2023**, *35*, 012103. [[CrossRef](#)]

Disclaimer/Publisher’s Note: The statements, opinions and data contained in all publications are solely those of the individual author(s) and contributor(s) and not of MDPI and/or the editor(s). MDPI and/or the editor(s) disclaim responsibility for any injury to people or property resulting from any ideas, methods, instructions or products referred to in the content.